Pipeline Leak Detection Using the Matched-Field Processing Method

Xun Wang[1] and Mohamed S. Ghidaoui, M.ASCE[2]

Abstract: A transient-based leakage detection method using a matched-field processing (MFP) scheme is formulated and applied. It is found to be efficient, robust, accurate, and provides a unique solution. Its inherent efficiency stems from the fact that the MFP method decouples the search for the leak location and the leak size. Its robustness is demonstrated by showing that the MFP method is able to estimate the location and size of leak in the presence of (1) noise even for signal-to-noise ratio (SNR) as low as SNR $= -3$ dB, and (2) uncertainty in the fluid–pipe system wave speed. Another positive attribute of the MFP method is that it is able to use all available frequencies, rather than just resonant frequencies, and does not need to identify resonant frequencies. As a result, the MFP method provides precise localization estimates even in noisy environments. It is also shown that a unique identification is achieved by the MFP method provided that the pressure signal is measured at two locations along the pipe. For the case of multiple leaks, MFP identifies each of the leaks provided that the distance between the leaks is of the same order or larger than the shortest probing half-wavelength. **DOI: 10.1061/(ASCE)HY.1943-7900.0001476.**

Author keywords: Leak detection; Transient wave; Water hammer; Inverse analysis; Matched-field processing; Noise; Uncertainty.

Introduction

Leak detection is an important issue in water supply systems because leakage results in financial losses from wastage of water, energy, and other process inputs used to treat the water. Leaks also pose health risks since leaks are potential entry points for contaminants during low-pressure intrusion events (Colombo et al. 2009). The World Bank estimates the worldwide monetary value of lost water at about USD 15 billion/year. The Asian Development Bank estimates that the value of water lost in Asia is USD 9 billion/year. These are direct water costs and do not account for indirect socioeconomic costs in which larger pipe failures can disrupt businesses, interrupt production processes, cause floods, and damage properties. Studies show that typical water loss in most countries ranges from 20 to 30% (Colombo et al. 2009). In addition, the 2003 report by the American Water Works Association (AWWA) Water Loss Control Committee estimates that 5–10 billion kWh of power generated each year in the United States is lost to unaccounted-for water.

Fluid transient-based defect detection methodology makes use of introduced hydraulic pressure wave(s) and their measured pressure response at specified location(s) to identify and localize various defects or anomalies in water pipe systems, such as leakages and blockages, including air blocks or tuberculated pipes and sediment deposition. The methods are a promising general approach for the detection of leaks and other defects. The basic premise of this approach to defect identification and characterization is that a measured pressure wave signal in the conduit fluid is modified by its interaction with the physical system components as it propagates and reflects throughout the system. Accordingly, it contains information, a sort of imprint of the conduits' properties and states. Specific methodological examples of this approach are (1) transient reflection-based method (TRM), such as Brunone (1999), Brunone and Ferrante (2001), and Covas et al. (2005b); (2) transient damping-based method (TDM) by Wang et al. (2002); (3) frequency response–based method (FRM) by Liou (1998), Mpesha et al. (2001), Ferrante and Brunone (2003), Covas et al. (2005a), Lee et al. (2003, 2005a, b, 2006), Sattar and Chaudhry (2008), Taghvaei et al. (2010), and Rubio Scola et al. (2016); and (4) inverse transient-based method (ITM) studied in Liggett and Chen (1994), Vítkovský et al. (2000), Stephens (2008), and Covas and Ramos (2010).

As evidenced in the foregoing literature, current implementations of fluid transient-based defect detection methods are robust for simple pipe systems in which the signal-to-noise ratio (SNR) is large and the values of model parameters are assumed to be either certain, or uncertain but exhibiting small variability. The real-world pipe environment, of course, contains myriad noise sources, e.g., turbulence, dynamic flow control and actuator devices, traffic, and many other activities. As a result, obtaining large SNRs often requires probing transient waves having significant amplitudes to identify defects. Such large amplitude transients are undesirable because they could compromise the structural integrity of pipes, especially when repeated many times for regular diagnostic tests of the pipe system. Presently, a transient-based methodology that can detect defects in a noisy environment with uncertain parameters is lacking.

Matched-field processing (MFP) is a signal processing methodology that is well suited for noisy environments and for problems with unknown and/or uncertain parameters (Jensen et al. 2000; Baggeroer et al. 1993). For example, MFP is a work horse of researchers, practicing scientists and engineers in ocean acoustics, and has been successfully used in many oceanic applications: to localize sound sources (e.g., enemy submarines, whales singing

[1]Research Associate, Dept. of Civil and Environmental Engineering, Hong Kong Univ. of Science and Technology, Clear Water Bay, Hong Kong, China (corresponding author). ORCID: https://orcid.org/0000-0002-1156-3840. Email: xunwang00@gmail.com

[2]Chinese Estates Professor of Engineering and Chair Professor, Dept. of Civil and Environmental Engineering, Hong Kong Univ. of Science and Technology, Clear Water Bay, Hong Kong, China. Email: ghidaoui@ust.hk

Note. This manuscript was submitted on February 17, 2017; approved on December 18, 2017; published online on April 16, 2018. Discussion period open until September 16, 2018; separate discussions must be submitted for individual papers. This paper is part of the ***Journal of Hydraulic Engineering***, © ASCE, ISSN 0733-9429.

in the ocean), to image the ocean's structure and topography, to localize munitions like mines, to infer unknown ocean model parameters, and to study ocean biology (Kuperman and Lynch 2004). The MFP approach has also been applied to source reconstruction in seismology (Corciulo et al. 2012) and structural vibration (Turek and Kuperman 1997), and for detecting damage in platelike structures (Hall and Michaels 2010; Tippmann et al. 2015). Tolstoy et al. (2009) and Tolstoy (2010) made an initial attempt to apply MFP to detect blockage in a sewer pipe. Note that in the last two works, the acoustic field in the pipe is not modeled such that some of the concerned parameters cannot be estimated. The present paper develops a transient model–based MFP approach for the detection of leaks in pipes in noisy environments.

This paper is a complete version of the results presented by the authors in Wang and Ghidaoui (2017). This paper begins by describing the pipe system and the hydraulic transient model. Then, the MFP method is introduced: the leak position and size are respectively estimated. Both white and nonwhite noises are considered. The performance of the proposed method for multiple leaks, as well as its resolution, is discussed. Then, the analytical properties of MFP are introduced. The proposed method is linked to a matched-filter approach which maximizes SNR. The physical meaning of MFP in the time domain is also explained. Numerical simulation results justify the estimation efficiency of MFP for both white and nonwhite measurement noise. A two-leak example and the resolution in terms of separating two leaks close together are discussed. The robustness of the proposed method with respect to imprecise wave speed is numerically investigated.

Leak Detection Using Matched-Field Processing

This section first presents the pipeline transient model considered in the paper. MFP is then introduced to solve the leakage detection problem. The single- and multiple-leak cases with white and nonwhite noise are both discussed.

Model

The pipeline configuration is illustrated in Fig. 1. A single pipe bounded by an upstream and a downstream node, whose coordinates are $x = x^U = 0$ and $x = x^D$, respectively. A sensor, whose coordinate is denoted by x^M, is assumed to be positioned near the downstream node. A single leak is assumed with leak location x^L ($x^L < x^M$), and Q_0^L and H_0^L are, respectively, the steady-state discharge and head at the leak. The leak size is represented by the lumped leak parameter $s^L = C^d A^L$, where C^d is the discharge coefficient of the leak and A^L is the flow area of the leak opening (orifice). The steady-state discharge of the leak is related to the lumped leak parameter by $Q_0^L = s^L\sqrt{2g(H_0^L - z^L)}$, in which g is the gravitational acceleration and z^L denotes the elevation of the pipe at the leak.

The discharge and head oscillations due to a fluid transient are represented by q and h. The linearized unsteady-oscillatory continuity and momentum equations in the time domain (Chaudhry 2014) are

$$\frac{a^2}{gA}\frac{\partial q}{\partial x} + \frac{\partial h}{\partial t} = 0 \tag{1}$$

$$\frac{1}{gA}\frac{\partial q}{\partial t} + \frac{\partial h}{\partial x} + Rq = 0 \tag{2}$$

for $x \in [x^U, x^L) \cup (x^L, x^D]$, where a = wave speed; A = area of pipeline; R = steady-state resistance term being $R = (fQ_0)/(gDA^2)$ for turbulent flows; f = Darcy–Weisbach friction factor; Q_0 = steady-state discharge in the pipe; and D = pipe diameter. Taking the Fourier transform of Eqs. (1) and (2) with respect to t gives q and h in the frequency domain

$$\frac{a^2}{gA}\frac{\partial q}{\partial x} + \mathrm{i}\omega h = 0 \tag{3}$$

$$\frac{\partial h}{\partial x} + \left(\frac{\mathrm{i}\omega}{gA} + R\right)q = 0 \tag{4}$$

where ω = angular frequency. Solving Eqs. (3) and (4) with boundary condition of the discharge $q(x^U)$ and head $h(x^U)$ at x^U and the head and mass conservation condition across the leak

$$h(x^{L-}) = h(x^{L+}) = h(x^L) \tag{5}$$

$$q(x^{L-}) = q(x^{L+}) + q(x^L) = q(x^{L+}) + \frac{Q_0^L}{2(H_0^L - z^L)}h(x^L) \tag{6}$$

in which x^{L-} and x^{L+} represent, respectively, just upstream and downstream of the leak; the quantities at x^M can be computed in the following way (Chaudhry 2014):

$$\begin{pmatrix} q(x^M) \\ h(x^M) \end{pmatrix} = M^{NL}(x^M - x^L) \times \begin{pmatrix} 1 & -\dfrac{Q_0^L}{2(H_0^L - z^L)} \\ 0 & 1 \end{pmatrix} M^{NL}(x^L)\begin{pmatrix} q(x^U) \\ h(x^U) \end{pmatrix} \tag{7}$$

In Eq. (7),

$$M^{NL}(x) = \begin{pmatrix} \cosh(\mu x) & -\dfrac{1}{Z}\sinh(\mu x) \\ -Z\sinh(\mu x) & \cosh(\mu x) \end{pmatrix} \tag{8}$$

is the field matrix, where the superscript NL stands for no leak; $Z = \mu a^2/(\mathrm{i}\omega gA)$ is the characteristic impedance; and $\mu = a^{-1}\sqrt{-\omega^2 + \mathrm{i}gA\omega R}$ is the propagation function. If the pipe is frictionless ($f = 0$), $\mu = \mathrm{i}k$, where $k = \omega/a$ is the wavenumber.

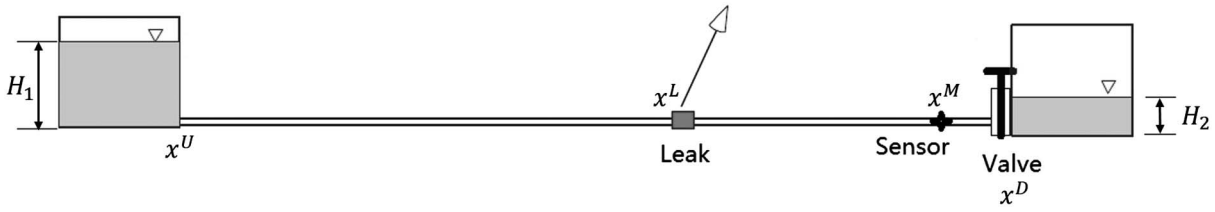

Fig. 1. Configuration of the considered pipeline system.

J. Hydraul. Eng., 2018, 144(6): 04018030

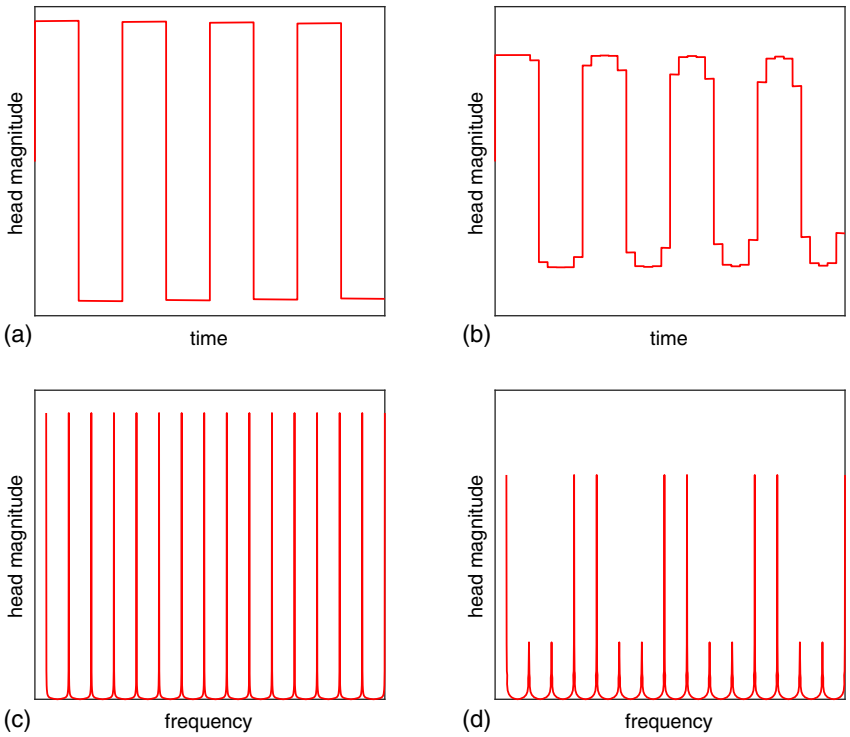

Fig. 2. Transient wave in the (a and b) time domain; and (c and d) frequency domain for (a and c) an intact pipe and (b and d) a leaking pipe.

Fig. 2 shows an example of transient wave signal in the time domain (with a step input signal due to a valve closure) and in the frequency domain (frequency response function) measured at x^D. It is clear that a leak modifies both signals. In the former, small jumps can be found due to the reflections at the leak. In the latter, the pressure head in the frequency domain damps the resonant frequencies in a periodic manner. This periodic pattern was used by Lee et al. (2005a, b) to propose a leak detection technique.

The transfer matrix on the right hand side of Eq. (7) can be simplified as

$$M^{NL}(x^M - x^L)\begin{pmatrix} 1 & -\dfrac{Q_0^L}{2(H_0^L - z^L)} \\ 0 & 1 \end{pmatrix} M^{NL}(x^L) = M^{NL}(x^M) + s^L M^{SL}(x^L) \tag{9}$$

in which

$$M^{SL}(x^L) = \sqrt{\frac{g}{2(H_0^L - z^L)}}\begin{pmatrix} Z\sinh(\mu x^L)\cosh(\mu(x^M - x^L)) & -\cosh(\mu x^L)\cosh(\mu(x^M - x^L)) \\ -Z^2\sinh(\mu x^L)\sinh(\mu(x^M - x^L)) & Z\cosh(\mu x^L)\sinh(\mu(x^M - x^L)) \end{pmatrix} \tag{10}$$

is a matrix related to the location x^L of the leak (z^L is determined by x^L) but independent of the leak size s^L.

By combining Eqs. (7)–(10), the head at $x = x^M$ for a given angular frequency ω is

$$h(\omega, x^M) = h^{NL}(\omega, x^M) + s^L G(\omega, x^L, x^M) \tag{11}$$

wherein

$$h^{NL}(\omega, x^M) = -Z\sinh(\mu x^M)q(x^U) + \cosh(\mu x^M)h(x^U) \tag{12}$$

and

$$G(\omega, x^L, x^M) = -\frac{\sqrt{g}Z\sinh(\mu(x^M - x^L))}{\sqrt{2(H_0^L - z^L)}}(Z\sinh(\mu x^L)q(x^U) - \cosh(\mu x^L)h(x^U)) \tag{13}$$

Let h_j^M denote the measured head at the frequency ω_j. The measurement is assumed to be contaminated by a noise n_j, that is,

$$h_j^M = h^{NL}(\omega_j, x^M) + s^L G(\omega_j, x^L, x^M) + n_j \tag{14}$$

The purpose of this work is to use the measured head at J frequencies, denoted as $\mathbf{h}^M = (h_1^M, \ldots, h_J^M)$, to estimate x^L (the leak location) and s^L (the leak size). Here, let us define the head difference due to leakage $\Delta\mathbf{h} = (\Delta h_1, \ldots, \Delta h_J)^\top$, where $\Delta h_j = h_j^M - h^{NL}(\omega_j, x^M)$ $(j = 1, \ldots, J)$, and denote $\mathbf{G}(x^L) = (G(\omega_1, x^L, x^M), \ldots, G(\omega_J, x^L, x^M))^\top$ and the error vector by $\mathbf{n} = (n_1, \ldots, n_J)^\top$. Then, the head difference is represented by

$$\Delta\mathbf{h} = s^L\mathbf{G}(x^L) + \mathbf{n} \tag{15}$$

Note that the noise is broadly classified into white and nonwhite (colored) noise. The former can be assumed if, in the concerned bandwidth, the energy at various frequencies does not significantly change or no prior information is available for noise structure. Nonwhite noise is more common in real-world pipeline applications in which the source of noise can be due to equipment

accuracy, turbulence, dynamic devices such as pumps, traffic, and so forth (Schantz et al. 2014; Hwang et al. 2009). In what follows, white noise is first dealt with and then the approach is generalized to the case of nonwhite noise through the use of noise whitening. The whitening scheme allows to apply the leakage detection technique to problem in which the noise is nonwhite but its distribution is known.

Leak Detection Using Matched-Field Processing with White Noise

The leakage localization problem is itself solved using the MFP method. The noise vector $\mathbf{n}$ is assumed to follow a zero-mean Gaussian distribution $\mathcal{N}(\mathbf{0}, \sigma^2\mathbf{I}_J)$, where $\mathbf{I}_J$ is a J-dimensional identity matrix. The key idea of MFP is to adjust a unit vector $\mathbf{w} = (w_1, \ldots, w_J)^\top$ ($|\mathbf{w}| = 1$) to have the same direction (in the J-dimensional complex vector space) as the measurement. The output function is defined by the inner product between the weighting vector $\mathbf{w}$ and the head difference $\Delta\mathbf{h}$

$$B \equiv < \mathbf{w}, \Delta\mathbf{h} >= \mathbf{w}^H \Delta\mathbf{h} \in \mathbb{C} \tag{16}$$

where the superscript H stands for the conjugate transpose. The optimal weight is obtained by solving for $\mathbf{w}$ which maximizes

$$|B|^2 = |\mathbf{w}^H \Delta\mathbf{h}|^2 = \mathbf{w}^H \Delta\mathbf{h}\Delta\mathbf{h}^H\mathbf{w} \tag{17}$$

By inserting Eq. (15) into Eq. (17) and maximizing its expectation (denoted by $\mathbb{E}$) with respect to $\mathbf{w}$, the optimal weight is obtained

$$\hat{\mathbf{w}} = \arg\max_{\mathbf{w}} \mathbb{E}(|B|^2) = \arg\max_{\mathbf{w}}((s^L)^2\mathbf{w}^H\mathbf{G}\mathbf{G}^H\mathbf{w} + \sigma^2)$$
$$= \arg\max_{\mathbf{w}}(\mathbf{w}^H\mathbf{G}\mathbf{G}^H\mathbf{w}) = \pm\frac{\mathbf{G}}{\sqrt{\mathbf{G}^H\mathbf{G}}} \tag{18}$$

in which argmax represents the argument of the maximum. Algebraically, the optimal $\mathbf{w}$ is a vector parallel to $\mathbf{G}$. Then, the leakage location can be estimated by substituting Eq. (18) back to Eq. (17)

$$\widehat{x^L} = \arg\max_{x^L} \frac{\Delta\mathbf{h}^H\mathbf{G}(x^L)\mathbf{G}^H(x^L)\Delta\mathbf{h}}{\mathbf{G}^H(x^L)\mathbf{G}(x^L)} \tag{19}$$

It is interesting, perhaps even remarkable, that Eq. (19) is also a maximum likelihood estimate (MLE) (Krim and Viberg 1996; Wang et al. 2016a, b) of the leak position and the leak size can be estimated by

$$\widehat{s^L} = \frac{\mathbf{G}^H(\widehat{x^L})\Delta\mathbf{h}}{\mathbf{G}^H(\widehat{x^L})\mathbf{G}(\widehat{x^L})} \tag{20}$$

A proof of the foregoing assertion can be found in Appendix I. According to the properties of MLE, Eqs. (19) and (20) are consistent estimators, i.e., they converge in probability to the actual values.

It has been diagrammatically indicated in Lee et al. (2005a) that the shape and magnitude of the frequency response diagram independently determine the location and the size of the leak. In the present paper, the location and size are separately estimated; Eq. (19) is first used to obtain the estimate $\widehat{x^L}$ of x^L and then this $\widehat{x^L}$ is inserted in Eq. (20) to estimate the leak size. Unlike existing techniques, the proposed method uses not only the resonant frequencies, but all the frequencies in between. This is important because (1) identification of resonant frequencies is challenging in practice, and (2) the use of all available frequencies improves the localization precision.

Whitening Signal Noise

The assumption of white noise may not apply in practice owing to systematic errors. For example, noise from turbulence, traffic, and hydraulic devices cannot be modeled by white noise. In this section, leak detection using measurements containing nonwhite noise is considered. Assuming that the noise structure is known, the measurement may be filtered such that the noise is whitened (Kessy et al. 2018). As a result, the method based on the white noise assumption can be used.

Here, the covariance matrix Σ of the noise vector $\mathbf{n} \sim \mathcal{N}(\mathbf{0}, \Sigma)$ is eigen-decomposed as

$$\Sigma = \Phi\Lambda\Phi^{-1} = \Phi\Lambda^{\frac{1}{2}}\Lambda^{\frac{1}{2}}\Phi^{-1} \tag{21}$$

where Λ = diagonal matrix with the eigenvalues of Σ on the diagonals; Φ = matrix of the corresponding eigenvectors; and $\Phi^{-1} = \Phi^H$. By applying a filter $\Lambda^{-1/2}\Phi^H$, the noise becomes

$$\tilde{\mathbf{n}} = \Lambda^{-\frac{1}{2}}\Phi^H\mathbf{n} \tag{22}$$

Note that the covariance matrix of $\tilde{\mathbf{n}}$ is

$$\mathrm{Cov}(\tilde{\mathbf{n}}) = \mathbb{E}(\tilde{\mathbf{n}}\tilde{\mathbf{n}}^H) = \mathbb{E}(\Lambda^{-\frac{1}{2}}\Phi^H\mathbf{n}\mathbf{n}^H\Phi\Lambda^{-\frac{1}{2}}) = \Lambda^{-\frac{1}{2}}\Phi^H\Sigma\Phi\Lambda^{-\frac{1}{2}} = \mathbf{I}_J \tag{23}$$

which implies that the noise is whitened.

Filtering the head difference by $\Lambda^{-1/2}\Phi^H$, it becomes

$$\widetilde{\Delta\mathbf{h}} = \Lambda^{-\frac{1}{2}}\Phi^H\Delta\mathbf{h} = s^L\Lambda^{-\frac{1}{2}}\Phi^H\mathbf{G}(x^L) + \Lambda^{-\frac{1}{2}}\Phi^H\mathbf{n} = s^L\tilde{\mathbf{G}}(x^L) + \tilde{\mathbf{n}} \tag{24}$$

where $\tilde{\mathbf{G}}(x^L) = \Lambda^{-1/2}\Phi^H\mathbf{G}(x^L)$. Then, the leak position and size can be estimated via Eqs. (19) and (20), where $\Delta\mathbf{h}$ and $\mathbf{G}$ are replaced by $\widetilde{\Delta\mathbf{h}}$ and $\tilde{\mathbf{G}}$, respectively.

Detecting Multiple Leaks

In the case of two leaks with location x^{L_i}, pipe elevation z^{L_i} at x^{L_i}, and size s^{L_i}, $i = 1, 2$, the measured head at x^M ($x^M > x^{L_2} > x^{L_1}$) is denoted by the expression

$$h^M(\omega) = h^{NL}(\omega) + s^{L_1}G(\omega, x^{L_1}) + s^{L_2}G(\omega, x^{L_2}) + s^{L_1}s^{L_2}G^{CE}(\omega, x^{L_1}, x^{L_2}) \tag{25}$$

in which

$$G^{CE}(\omega, x^{L_1}, x^{L_2}) = \frac{gZ^2\sinh(\mu(x^{L_2} - x^{L_1}))\sinh(\mu(x^M - x^{L_2}))}{2\sqrt{(H_0^{L_1} - z^{L_1})(H_0^{L_2} - z^{L_2})}} \times(-Z\sinh(\mu x^{L_1})q(x^U) + \cosh(\mu x^{L_1})h(x^U)) \tag{26}$$

represents the coupling effect of the two leaks. The derivation of Eq. (25) can be found in Appendix II. For small leaks, i.e., $s^{L_i} \ll 1$, the contribution of the last term of Eq. (25) is much smaller than the other terms, and thus may be ignored. Therefore, the head difference $\Delta\mathbf{h} = (h_1^M - h_1^{NL}, \ldots, h_J^M - h_J^{NL})^\top$ can be approximated by

$$\Delta\mathbf{h} \approx \Delta\mathbf{h}_1 + \Delta\mathbf{h}_2 = s^{L_1}\mathbf{G}(x^{L_1}) + s^{L_2}\mathbf{G}(x^{L_2}) \tag{27}$$

In the presence of multiple leaks, the localization method based on the assumption of single leak can still be used. Consider two leaks with same leak size s^{L_i}, the output function is a superposition of the contributions from the two leaks

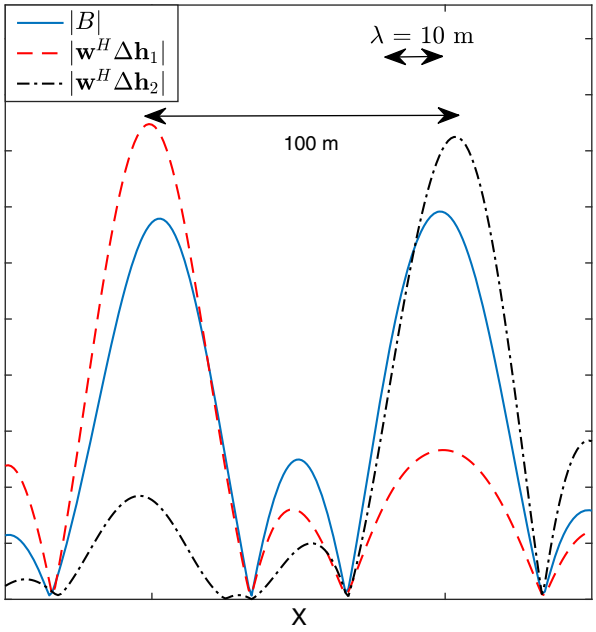

Fig. 3. Superposition of two output functions of MFP corresponding to two leaks.

$$B(x) = \mathbf{w}^H\Delta\mathbf{h} \approx \mathbf{w}^H\Delta\mathbf{h}_1 + \mathbf{w}^H\Delta\mathbf{h}_2 = \frac{\mathbf{G}^H(x)}{\sqrt{\mathbf{G}^H(x)\mathbf{G}(x)}}\mathbf{G}(x^{L_1}) + \frac{\mathbf{G}^H(x)}{\sqrt{\mathbf{G}^H(x)\mathbf{G}(x)}}\mathbf{G}(x^{L_2}) \quad (28)$$

When two leaks are not close to each other, the output (merit) function has two local maxima that correspond to the two leak positions. Fig. 3 shows an example of the superposition of two output functions, in which the distance between the two leaks is 100 m and the minimum wavelength is around 10 m. In Fig. 3, the width of each main lobe (corresponding to the output function of each leak) is much smaller than the distance between leaks, allowing the two leaks to be clearly identified. However, when two leaks are close to each other, the superposition only exposes one maximum which locates between the two actual leak locations. For example, moving $|\mathbf{w}^H\Delta\mathbf{h}_1|$ and $|\mathbf{w}^H\Delta\mathbf{h}_2|$ in Fig. 3 together would mix the two local maxima. The resolution, which is defined as the minimum distance between the two leaks that can be resolved, depends on the maximum frequency (or minimum wavelength) of the probing wave. According to the spatial Nyquist criterion, the resolution limit is equal to the minimum probing half-wavelength.

The MFP leak detection algorithm is described in Algorithm 1.

Algorithm 1. Leak detection using MFP

1. Select J frequencies $\omega_1, \ldots, \omega_J$ for leak detection.
2. Calculate $h_1^{NL}, \ldots, h_J^{NL}$ at the frequencies $\omega_1, \ldots, \omega_J$ via Eq. (11) and use the head differences $\Delta h_j = h_j^M - h_j^{NL}$ $(j = 1, \ldots, J)$ as the data.
3. If the measurement noise is nonwhite, filter the head difference by Eq. (24).
4. Plot $|B|^2$ [Eq. (19)] with respect to x^L and see the local maxima with relatively high magnitudes as the candidates of leak estimate.
5. Repeat Steps 1–4 with another measurement station, if each local maximum in Step 4 is still a local maximum of $|B|^2$ for the new measurement point, retain it as a leak estimate.
6. If the source number (decided in Step 5) is one, estimate the leak size from Eq. (20).

Analytical Properties of the Matched-Field Processing Method

In this section, the analytical properties of the proposed MFP method are presented. MFP is shown to be equivalent to an optimal filter that maximizes SNR. An interpretation of the MFP method in the time domain is also given.

Optimal Filter Maximizing SNR

The output function of MFP [Eq. (16)] is equivalent to applying a filter $\mathbf{w}^H$ to the head difference $\Delta\mathbf{h}$

$$\mathbf{w}^H\Delta\mathbf{h} = s^L\mathbf{w}^H\mathbf{G} + \mathbf{w}^H\mathbf{n} \quad (29)$$

The optimal filter can be determined by maximizing SNR

$$\max\frac{|s^L\mathbf{w}^H\mathbf{G}|^2}{\mathbb{E}(|\mathbf{w}^H\mathbf{n}|^2)} = \max\frac{(s^L)^2|\mathbf{w}^H\mathbf{G}|^2}{\sigma^2|\mathbf{w}|^2} \quad (30)$$

The filter maximizing Eq. (30) (with the constraint $|\mathbf{w}| = 1$) is

$$\hat{\mathbf{w}} = \frac{\mathbf{G}}{\sqrt{\mathbf{G}^H\mathbf{G}}} \quad (31)$$

which is identical with Eq. (18). This property shows that MFP minimizes the influence of noise and is thus robust in a noisy environment.

MFP in the Time Domain

Since the operation of a complex conjugate in the frequency domain is equivalent to the time reversal in the time domain (Khazaie et al. 2016) (Appendix III), Eq. (16) can be rewritten

$$B = \sum_{j=1}^{J} w_j^c(\omega_j)\Delta h(\omega_j) = \sum_{j=1}^{J}\mathcal{F}_{\omega_j}(W(T-t+1))\mathcal{F}_{\omega_j}(\Delta H(t)) = \sum_{j=1}^{J}\mathcal{F}_{\omega_j}(W(T-t+1) * \Delta H(t)) \quad (32)$$

where the asterisk stands for the convolution; $\mathcal{F}_{\omega_j}$ represents the Fourier transform at ω_j; and $W(t)$ and $\Delta H(t)$, $t = 1, \ldots, T$ are the inverse Fourier transform of w and Δh. Note that $W(T-t+1) * \Delta H(t)$ is a filtering operation where W is the filter. Since the angular frequency can be arbitrarily taken, maximizing the output function with respect to $\mathbf{w}$ in the frequency domain is equivalent to finding an optimal filter in the time domain (the matched-filter method). It has been shown in Eq. (31) that the optimal $\mathbf{w}$ is the normalized theoretical expression of the head difference; therefore, the optimal filter is the convolution with the time-reversed head measurement in the time domain, that is,

$$W(T-t+1) * \Delta H(t) = \Delta H(T-t+1) * \Delta H(t) \quad (33)$$

Therefore, the MFP method can be understood as filtering the measured time signal such that the sound power is maximized. Physically, Eq. (33) corresponds to (weighted) hearing, i.e., recording sound waves only at the moments when the reflected waves arrive at the measurement station and being deaf at other times.

Numerical Simulation

In this section, numerical examples are introduced to test the MFP method. The case of a single leak with white and nonwhite noise

and the case of multiple leaks are respectively considered. The robustness of the proposed method with respect to uncertain fluid–pipe system wave speed is also investigated.

Single Leak with White Noise

First, the case of a single leak and white noise is considered. The leakage problem in a single pipeline is numerically simulated. The system arrangement is shown in Fig. 1. Two reservoirs are connected by a pipe in a horizontal plane; the heads of the upstream and downstream reservoirs are $H_1 = 25$ m and $H_2 = 20$ m, respectively. The pipe length is $l = 2{,}000$ m and the diameter is $D = 0.5$ m. The Darcy–Weisbach friction factor of the pipe is $f = 0.02$ and the steady-state discharge is $Q_0 = \sqrt{2\ gDA^2(H_1 - H_2)/(lf)} = 0.0153\ \text{m}^3/\text{s}$. The wave speed is $a = 1000$ m/s. A valve is located at the downstream end of the pipe and a pressure sensor is situated just upstream of the valve. It is assumed that an impulse wave is generated by rapidly closing and opening the valve, giving the boundary conditions $q(x^D) = 1$. The reservoir boundary condition at x^U is $h(x^U) = 0$. The wave propagation simulation in the frequency domain is accomplished using the transfer matrix method in Eq. (7). Note that the proposed MFP method is not limited to the impulse wave but can be applied to different types of valve maneuver or wave generation. Of course, like any other method, the sharper the transient, the higher would the resolution be. In addition, the fact that the proposed method uses all frequencies and not just resonant frequencies means that it is more robust than other methods even for a given maneuver.

The discharge at the upstream boundary is assumed to be obtained by measuring the head near the upstream reservoir. This approach is investigated in detail in Kashima et al. (2013) and is found to be in good agreement with experiments. Gaussian white noise with zero mean is added to both the head at x^M and the discharge at x^U. Here, the SNR in decibel is 10 dB, defined as

$$\text{SNR} = 20\log_{10}(\overline{|\mathbb{E}(\Delta\mathbf{h})|}/\sigma) = 20\log_{10}\left(\frac{s^L}{\sigma}\overline{|\mathbf{G}|}\right) \tag{34}$$

where $\overline{|\mathbb{E}(\Delta\mathbf{h})|}$ = average head difference; and σ = standard deviation of the Gaussian white noise. It is important to note that $\overline{|\mathbb{E}(\Delta\mathbf{h})|}/\sigma$ in Eq. (34) is the ratio between the average change of signal due to the leak (reflection and damping). Therefore, increasing SNR is equivalent to increasing the leak size s^L or decreasing the noise level σ. Another coefficient that affects the localization accuracy is the steady-state pressure head at the leak H_0^L (Liou 1998; Ferrante et al. 2014). It can be seen from Eqs. (11) and (13) that when $z^L = 0$ (the case studied in this section), H_0^L is proportional to s^L. Therefore, the influence of H_0^L can be equivalently quantified by varying SNR. For the aforesaid reasons, this section shows the simulation results with different SNR, but s^L and H_0^L are fixed.

Here, the case of single leak is considered; the leak location is $x^L = 400$ m and the lumped leak parameter (effective leak size) is $s^L = 1.4 \times 10^{-4}\ \text{m}^2$. The measurement location is at $x^M = 2{,}000$ m. The peak angular frequencies $\omega = n\omega_{th}, n = 1, 3, \ldots, 31$, are used for the leak localization, where $\omega_{th} = a\pi/(2l) = 0.94$ rad/s is the resonant frequency. Fig. 4(a) plots the power output $|B|^2$, which reaches maximum at the actual leak position (marked by the vertical dashed line). However, a symmetric maximum of $|B|^2$ having the same level can be found at $x = 1600$ m. This is due to the fact that $\mathbf{G}(x^L)$ is symmetric with respect to $x^M/2$ for the case $h(x^U) = 0$ [Eq. (13)], which implies that $|B|^2$ reaches

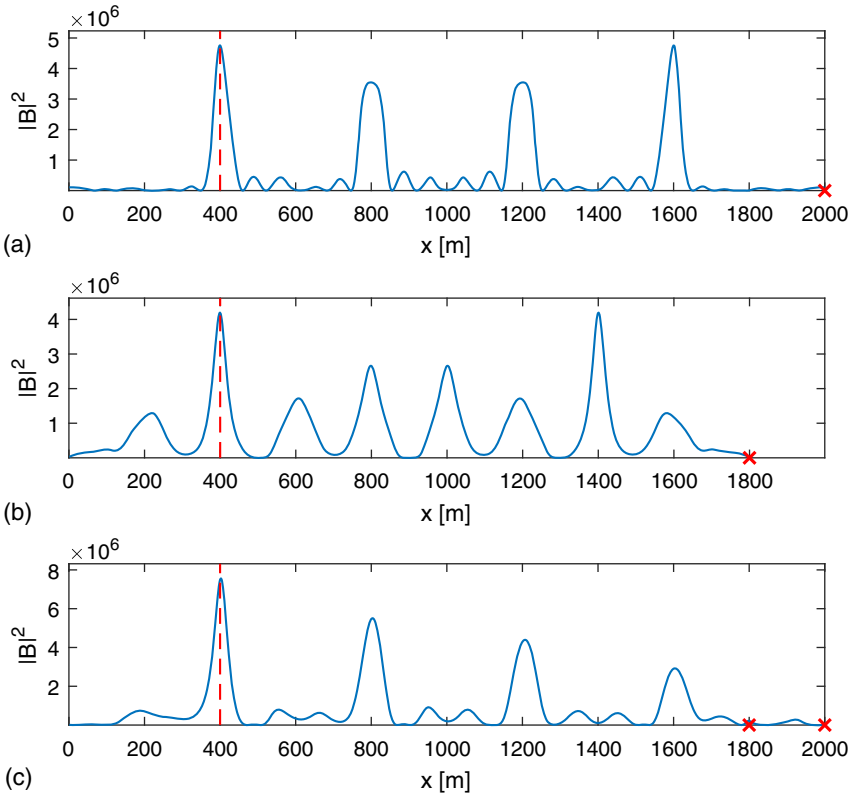

Fig. 4. Localization of a single leak using MFP (by plotting $|B|^2$) with (a) a single sensor at 2,000 m; (b) a single sensor at 1,800 m; and (c) two sensors at 1,800 and 2,000 m. The dashed lines and the crosses stand for the leak and sensor locations, respectively.

J. Hydraul. Eng., 2018, 144(6): 04018030

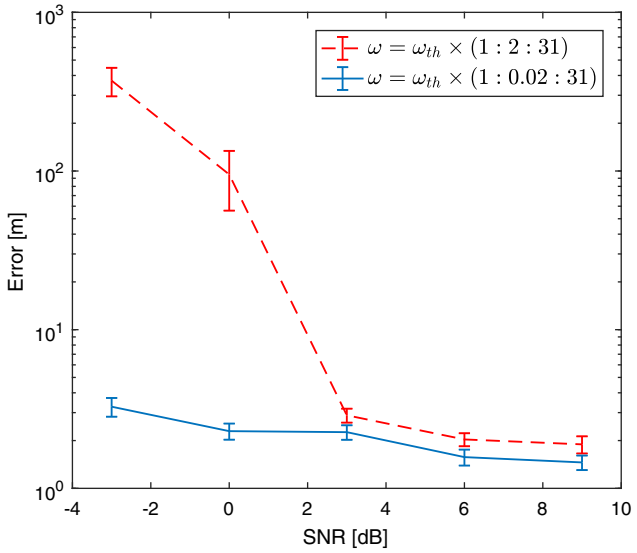

Fig. 5. Localization error of a single leak versus SNR. The used frequencies are $\omega = \omega_{th} \times (1{:}2{:}31)$ (only resonant frequencies) and $\omega = \omega_{th} \times (1{:}0.02{:}31)$, respectively.

maximum at both x^L and $x^M - x^L$. The issues of false (nonunique) localization and side lobes are resolved by adding another measurement station. By repeating the procedure but for $x^M =$ 1,800 m, it is found that the maximum at actual x^L remains at the original (and correct) location while the symmetric (false) maximum (as well as the other local maxima) moves and can thus be excluded [Fig. 4(b)]. Alternatively, if the data from both sensors are used simultaneously, the output function of MFP shows a unique maximum at the actual leak, as is illustrated in Fig. 4(c). Furthermore, the leak size s^L can be estimated via Eq. (20), which is $\widehat{s^L} = 1.41 \times 10^{-4}$ m^2 and is very close to its actual value 1.4×10^{-4} m^2 (the relative error is 0.7%).

The localization error with respect to various SNR (being -3, 0, 3, 6, and 9 dB, which correspond to the ratio $\overline{|\mathbb{E}(\Delta \mathbf{h})|}/\sigma$ between the average change of signal due to the leak and the average noise level ranging from 0.7 to 2.8) is shown in Fig. 5. The dashed line and solid line correspond to using the 16 peak frequencies $\omega = \omega_{th} \times (1{:}2{:}31)$ and more frequencies $\omega = \omega_{th} \times (1{:}0.02{:}31)$, respectively. Since the noise generation is random, the error shown in the figure is the average of 20 simulations, and the corresponding 95% confidence intervals are also displayed. It is obvious that for SNR not higher than 3 dB, both estimates are precise (the error is less than 3 m). For low SNR equal to 0 or -3 dB, however, only using peak frequencies leads to a large localization error. By contrast, using more frequencies can largely improve the estimate, the corresponding localization error is acceptable (always less than 5 m in this case).

The leak localization with various actual leak locations is also tested, which ranges from $x^L = 100$ to 1,700 m. Two sensors located at 1,800 and 2,000 m are used. As a matter of fact, in the case of high noise level, the cost function of MFP might be contaminated such that a side lobe is higher than the main lobe corresponding to the actual leak [Fig. 4(c)] and the locations of side lobes (and thus their distance to the actual leak) strongly depend on the actual leak location. In order to have a fair comparison for localization accuracy for different actual leak locations, the successful rate of localization, instead of the error, is thus computed. More specifically, for each case of SNR (0 and 6 dB) and selected frequencies [$\omega = \omega_{th} \times (1{:}2{:}31)$ and $\omega = \omega_{th} \times (1{:}0.02{:}31)$], the simulation is repeated 100 times and the successful rate, which is defined by the absolute error less than 10, 5, and 2 m (corresponding to $0.04\lambda_{\min}$, $0.02\lambda_{\min}$, and $0.01\lambda_{\min}$, where $\lambda_{\min}$ is the minimum wavelength), is computed and plotted in Fig. 6. Unsurprisingly, using more frequencies and higher SNR both lead to a higher successful rate of leak localization. In the case of using more frequencies [Figs. 6(b and d)], the localization accuracy is satisfactory considering that the error is much lower than the minimum half-wavelength of the used transient wave, i.e., $\lambda_{\min}/2 =$ 129 m. Furthermore, the successful rates versus leak location for error less than 5 and 2 m are irregular although a leak near the middle of the pipe seems slightly easier to be localized.

Single Leak with Nonwhite Noise

A numerical example for the case of nonwhite noise is considered here. The numerical setup is the same as in the previous case except that the noise vector $\mathbf{n}$ is assumed to be a blue noise, whose power density increases 3 dB per increasing frequency over the frequency range. First, the SNR at the first resonant frequency ω_{th} is assumed to be $\text{SNR}_1 = 30$ dB; the SNR at $31\omega_{th}$ is thus -55 dB. Figs. 7(a and b) display the output function of MFP before and after whitening the noise. Here, two measurement stations at 1,800 and 2,000 m are used. In this former case, since the noise distribution is nonwhite which does not meet the model assumption, the MFP method does not work efficiently. However, by whitening the blue noise, the MFP approach is able to find the maximum value at the actual leak location.

The leak localization error with respect to various SNR using different frequencies is investigated, as is shown in Fig. 8. The SNR at the first resonant frequency is $\text{SNR}_1 = 20$, 35, 50, 65, and 80 dB (the corresponding SNR at $31\omega_{th}$ is -65, -50, -35, -20, and -5 dB). In order to reduce the influence of randomness, the error is averaged by 20 simulations. As SNR decreases, the error in leak localization estimates without whitening noise dramatically increases while whitening the noise keeps errors at a comparable level (around 10 m when $\text{SNR}_1 = 20$ dB). Besides, using more frequencies $\omega = \omega_{th} \times (1{:}0.2{:}31)$, instead of only peak frequencies, also increases the precision of leak detection, as was indicated in the previous case of white noise.

Multiple Leaks

In this section, numerical simulations for the two-leak case are considered. First, two leaks are located at $x^{L_1} = 700$ m and $x^{L_2} =$ 1,600 m and the lumped leak parameters for both leaks are $s^{L_1} = s^{L_2} = 1.4 \times 10^{-4}$ m^2. The wave propagation is simulated, and the pressure heads obtained at $x =$ 1,800 and $x =$ 2,000 m constitute the measured heads. The noise is assumed to be white noise with SNR being 10 dB. The results using measurement (1) at $x =$ 1,800 m, (2) at $x =$ 2,000 m, and (3) at both $x =$ 1,800 and $x =$ 2,000 m are displayed in Fig. 9. It is clear that a single sensor is able to localize both leaks, but two symmetric maxima of $|B|^2$ appear as the single leak case. Again, using another sensor permits exclusion of the two false estimates: the two peaks of $|B|^2$ corresponding to the actual leaks remain while the other two move. Fig. 9(c) shows the result that uses both sensors in Figs. 9(a and b), in which the two highest maxima correspond to the two actual leaks.

In this example, two leaks can be separated by plotting $|B|^2$. However, the resolution depends on the distance between the leaks and the probing wavelength. In the following, two close leaks, whose coordinates are $x^{L_1} = 640$ m and $x^{L_2} = 700$ m, are considered. Since it has been shown that the symmetric leak estimates can

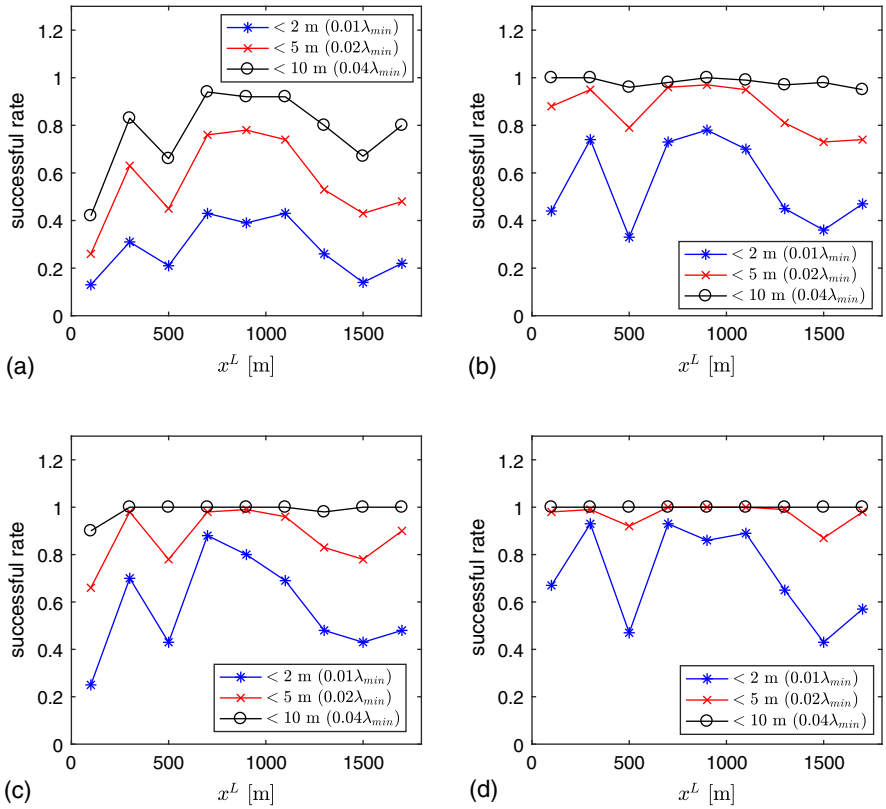

Fig. 6. Localization successful rate (defined by error less than 2, 5, and 10 m, respectively) of single leak with respect to various leak location. The frequencies used in the localization algorithm are, respectively (a and c) $\omega = \omega_{th} \times (1{:}2{:}31)$; and (b and d) $\omega = \omega_{th} \times (1{:}0.02{:}31)$. The SNR is (a and b) 0 dB; and (c and d) 6 dB.

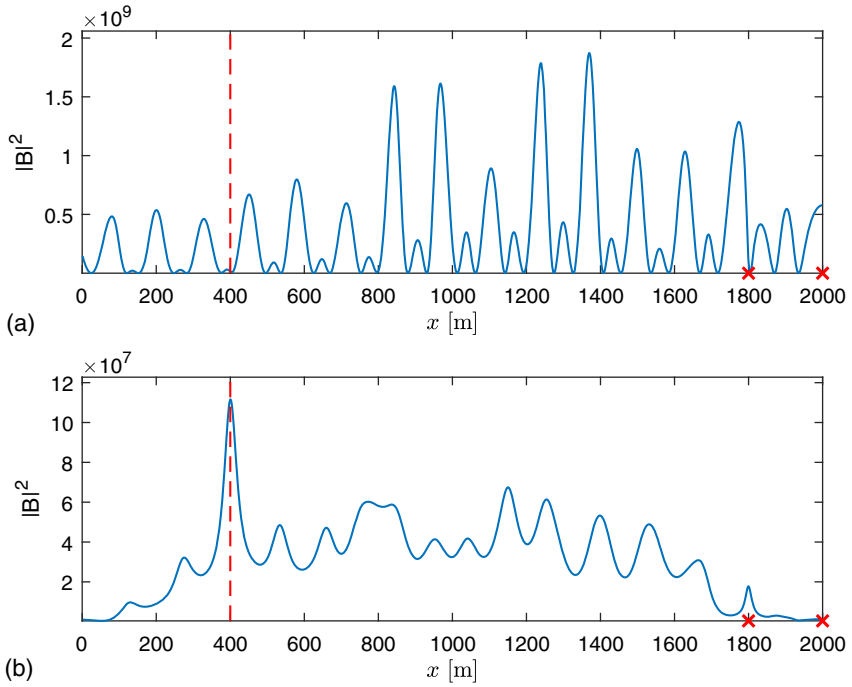

Fig. 7. Localization of a single leak using MFP (a) with whitening; and (b) without whitening the noise. The measurement noise follows a blue noise with $\text{SNR}_1 = 30$ dB at the first frequency. The dashed line and the cross stand for the leak and measurement locations, respectively.

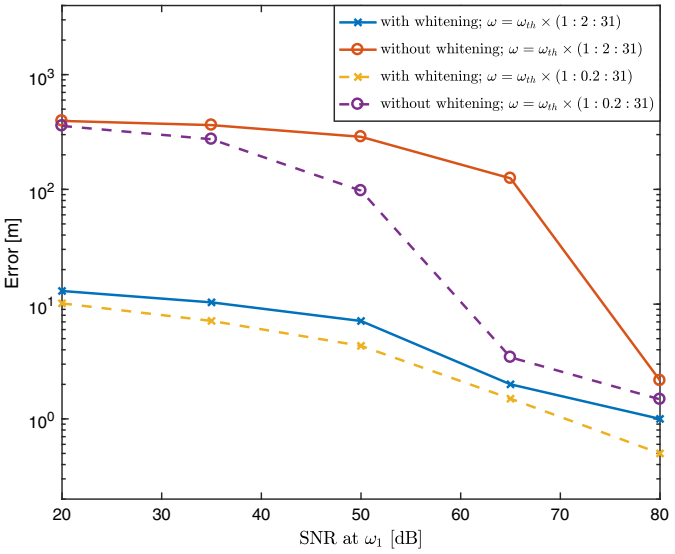

Fig. 8. Localization error of a single leak with and without whitening the blue noise. The frequencies used in the MFP method are $\omega = \omega_{th} \times (1{:}2{:}31)$ or $\omega = \omega_{th} \times (1{:}0.2{:}31)$.

be excluded by a secondary sensor, only the first half pipe is plotted. The first 16 peak frequencies ($\omega = n\omega_{th}, n = 1, 3, \ldots, 31$) are used for MFP, and the results are shown in Fig. 10(a). In this case, the minimum wavelength is $\lambda = 258$ m, i.e., the distance between leaks (60 m) is smaller than the minimum half-wavelength (129 m), thus the two leaks are not separated and only one maximum can be seen in the plot. Then, the maximum angular frequency is increased to $51\omega_{th}$ and $61\omega_{th}$ (the corresponding minimum wavelengths are, respectively, 157 and 131 m), the corresponding leak localization results are displayed in Figs. 10(b and c). In the former case, the minimum half-wavelength (78.5 m) is slightly larger than the leak distance; two local maxima can be found but both lobes are not totally separated. In the latter case, the minimum half-wavelength (65.5 m) is almost equal to the leak distance and the two leaks are resolvable. Furthermore, Fig. 10(c) exposes some side lobes. However, using more frequencies in the MFP method can suppress these side lobes. Fig. 10(d) plots the power output in which the frequency range is the same as Fig. 10(c), but more frequencies (between the peak frequencies) are used: $\omega = \omega_{th} \times (1{:}0.02{:}61)$. In this figure, the magnitudes of the side lobes are much lower than the former case. Note that $61\omega_{th} = 0.94 \times 61 \approx 57$ rad/s or 9 Hz. This calls for a valve maneuver of 0.1 s which is easily realized in practice.

Sensitivity with Uncertain Wave Speed

In this section, sensitivity of the proposed leakage detection method with respect to wave speed uncertainty is investigated. In physical experiments, the wave speed in a pipe may typically vary in a given pipe system by 10–15% (Wylie and Streeter 1978), which could potentially seriously affect the leakage detection estimates. Fig. 11 shows the frequency response of head at the valve with unit input discharge perturbation, for wave speeds of $a = 990$, 1,000, and 1,010 m/s respectively. Here, the pipe length is $l =$ 2,000 m, the leak location is $x^L = 400$ m and the lumped leak parameter $s^L = 1.4 \times 10^{-4}$ m^2. The location of measurement station is $x = 2{,}000$ m and the SNR is 10 dB. Fig. 11 illustrates that a slight variation of wave speed changes the resonant frequency, the peak frequencies, and, more importantly, the magnitude and sequence of the peaks, which may result in a strong sensitivity of leakage localization estimates.

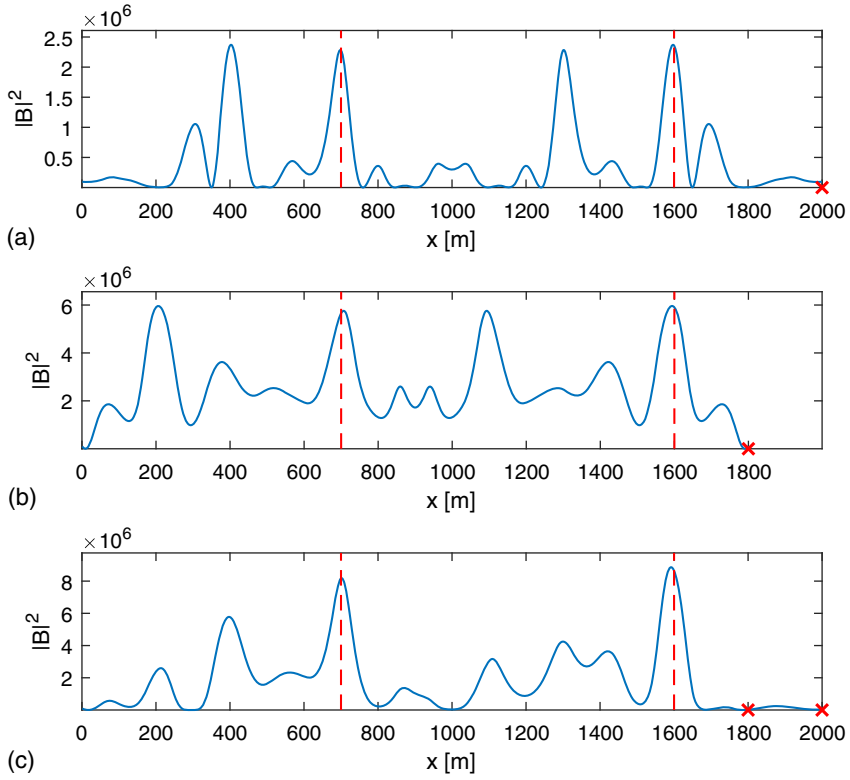

Fig. 9. Localization of two leaks using MFP with (a) a single sensor at 2,000 m; (b) a single sensor at 1,800 m; and (c) two sensors at 1,800 and 2,000 m. The dashed lines and the cross stand for the leak and sensor locations, respectively.

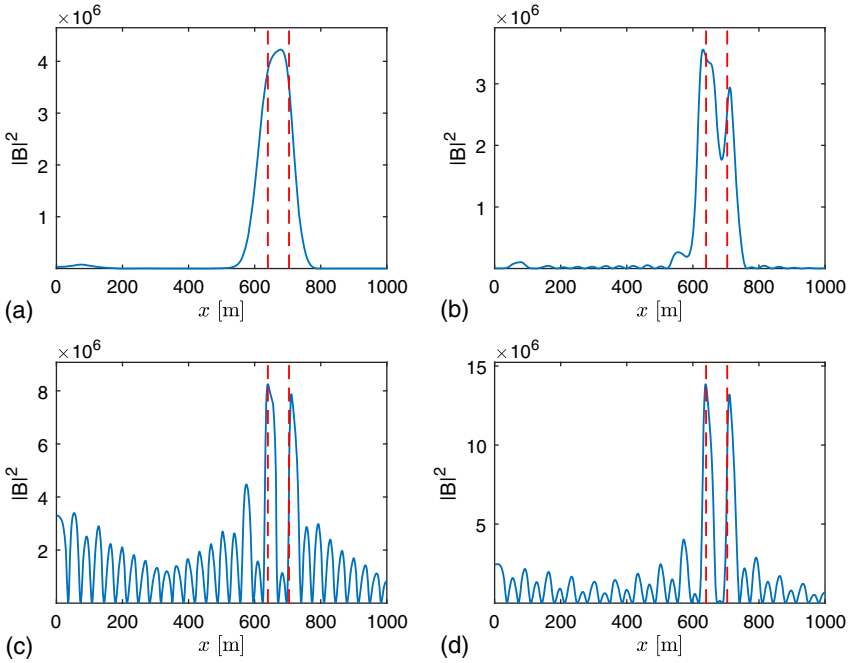

Fig. 10. Localization of two close leaks using MFP. The dashed lines stand for the locations of the leaks. The used maximum frequency is (a) $31\omega_{th}$; (b) $51\omega_{th}$; and (c and d) $61\omega_{th}$. In (a)–(c), only resonant frequencies are used; and in (d) more frequencies [$\omega = \omega_{th} \times (1{:}0.02{:}61)$] are used.

Fig. 12 displays the leak detection results with wave speed uncertainties: the assumed wave speed (which is a known parameter in the inverse problem) is 1,000 m/s while the actual wave speed in the forward problem (the simulation for measurement generation) is 850, 860, ..., 1,150 m/s, i.e., the error range is 15%. First, 16 peak frequencies $\omega = \omega_{th} \times (1{:}2{:}31)$ are used for the leak detection. Fig. 12(a) shows that when the error is smaller than 50 m/s (relative error of 5%), the estimation error is acceptable, but beyond this range the localization estimate exhibits a large jump, approximately from $\widehat{x^L} = 400$ to 800 m. The reason is that the high uncertainty level distorts the output function so that the side lobe of $|B|^2$ at 800 m becomes higher than the main lobe at 400 m [Fig. 4(a)], which therefore leads to an incorrect estimate. However, as previously shown in Figs. 10(c and d), using more frequencies is able to suppress the side lobes, which can thus solve the problem. Here, the angular frequencies $\omega = \omega_{th} \times (1{:}0.02{:}31)$ are used, which generate a more robust estimation result: the side lobe of $|B|^2$ no longer exceeds the main lobe. When the wave speed error increases to 150 m/s (15% relative error), the MFP method has an error of approximately 100 m, since the wrong information of wave speed leads to a wrong estimate of reflecting time from the leak. However, a smaller error interval of wave speed results in an acceptable error of leak localization. Fig. 12(b) illustrates that the estimation error is smaller than 5 m (the range is labeled by the dashed lines) when the wave speed error range is approximately ±35 m/s (3.5% relative error), using the frequencies $\omega = \omega_{th} \times (1{:}0.02{:}31)$. Again, only using peak frequencies [$\omega = \omega_{th} \times (1{:}2{:}31)$] generates a higher error: the localization error is around 8 m in the case that the wave speed error is 20 m/s (2% relative error).

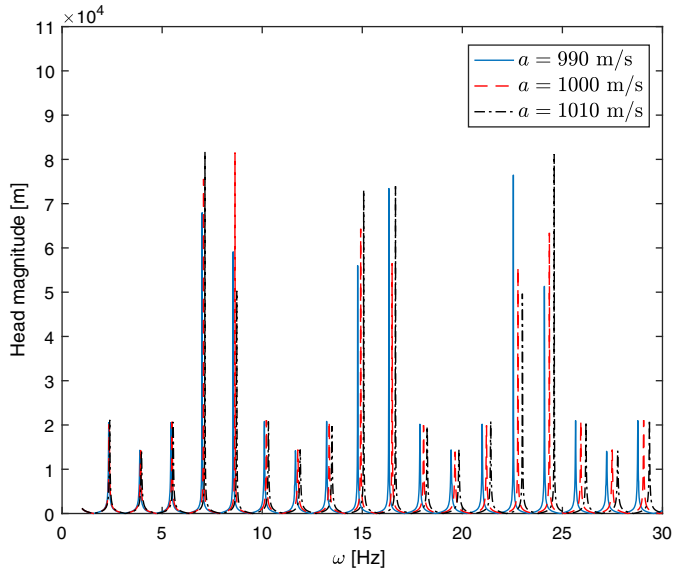

Fig. 11. Head response at $x^M = 2{,}000$ m in the frequency domain with unit input discharge perturbation at the valve with different wave speed $a = 990$, 1,000, and 1,010 m/s. The leak location is at $x^L = 400$ m.

Conclusions

This paper addresses the problem of leak detection in a pipeline using a fluid transient probing wave. A matched-field processing method is proposed to estimate the leak location and size. The estimate is proved to be a maximum likelihood estimate and it is explained by a matched-filter approach in both time and frequency domains. The measurement noise can be either white or nonwhite: in the latter case the noise has to be filtered by applying a whitening filter to the measurement of pressure head. The model is based on the single leak assumption but multiple leaks can still be localized due to the linear relationship of head difference contributions from various leaks. The proposed method is able to use the measurements at all available frequencies, rather than only peak

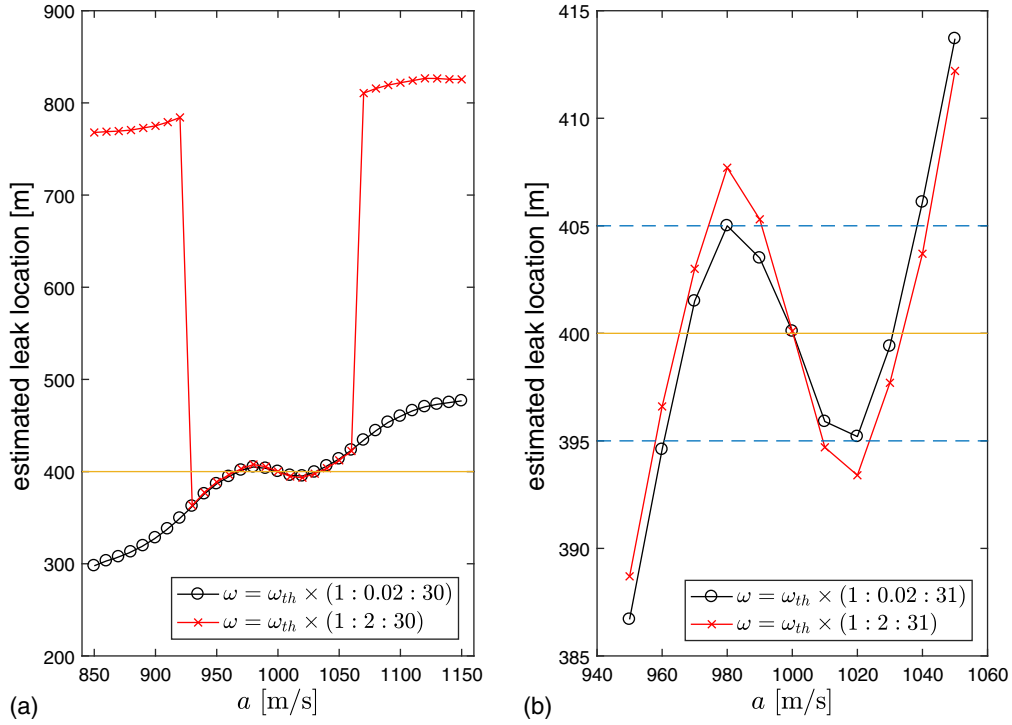

Fig. 12. Leak localization with imprecise wave speed. The assumed wave speed in the localization process is 1,000 m/s. The actual wave speed is (a) $a \in [850,\ 1{,}150]$ m/s; and (b) $a \in [950, 1{,}050]$ m/s. The angular frequency used in the MFP method is $\omega = \omega_{th} \times (1{:}2{:}31)$ or $\omega = \omega_{th} \times (1{:}0.02{:}31)$. The actual leak location is $x^L = 400$ m.

frequencies, which can improve the robustness and accuracy of leak estimates.

The results obtained from simulated data illustrate the potential utility of the proposed MFP method. The accuracy of the leak localization and the ability to resolve two leaks separated by a distance larger than minimum half-wavelength are demonstrated. The robustness with respect to measurement noise and imprecise wave speed is also investigated.

Future work may be conducted in several directions. A more complex model including uncertainty information on wave speed distribution would be interesting, which may further improve the leak detection accuracy. The influence of sensor location and the sensor distribution design for the multisensor case in both single pipe and branch system are worth studying. Furthermore, the present work deals with the localization of multiple leaks using a single-leak model. In order to further increase the estimation accuracy, robustness and the resolution, a model parametrizing the locations and sizes of multiple leaks may be considered. This latter approach is currently under development by the authors.

Appendix I. Maximum Likelihood Estimation of Leak Location and Size

It is assumed that the random error vector follows a complex-valued Gaussian distribution (Picinbono 1996) with zero mean and covariance matrix $\sigma^2 \mathbf{I}_J$, in which $\mathbf{I}_J$ is J-dimensional identity matrix. After removing unnecessary terms that are independent of the unknown parameters, the log-likelihood function of $\Delta\mathbf{h}$ is

$$L(x^L, s^L; \Delta\mathbf{h}) = -\|\Delta\mathbf{h} - s^L\mathbf{G}(x^L)\|^2 \tag{35}$$

Then, the MLE of leak location x^L and leak size s^L are given by

$$\left\{\widehat{x^L}, \widehat{s^L}\right\} = \arg\min_{x^L, s^L} \|\Delta\mathbf{h} - s^L\mathbf{G}(x^L)\|^2 \tag{36}$$

For any given leak location x^L, the MLE of s^L is a least square solution of Eq. (36)

$$\widehat{s^L} = \frac{\mathbf{G}^H(x^L)\Delta\mathbf{h}}{\mathbf{G}^H(x^L)\mathbf{G}(x^L)} \tag{37}$$

Inserting Eq. (37) into Eq. (36), the MLE of x^L are derived

$$\widehat{x^L} = \arg\min_{x^L} \left\|\Delta\mathbf{h} - \frac{\mathbf{G}(x^L)\mathbf{G}^H(x^L)}{\mathbf{G}^H(x^L)\mathbf{G}(x^L)}\Delta\mathbf{h}\right\|^2 \tag{38}$$

$$= \arg\max_{x^L} \frac{\Delta\mathbf{h}^H\mathbf{G}(x^L)\mathbf{G}^H(x^L)\Delta\mathbf{h}}{\mathbf{G}^H(x^L)\mathbf{G}(x^L)} \tag{39}$$

Appendix II. Theoretical Expression of Head Measurement in the Case of Double Leaks

In the case of double leaks, the discharge $q(x^M)$ and head $h(x^M)$ at x^M are given by

$$\begin{pmatrix} q(x^M) \\ h(x^M) \end{pmatrix} = M \begin{pmatrix} q(x^U) \\ h(x^U) \end{pmatrix} \tag{40}$$

wherein the transfer matrix is

$$M = M^{NL}(x^M - x^{L_2}) \begin{pmatrix} 1 & \dfrac{-Q_0^{L_2}}{2(H_0^{L_2} - z^{L_2})} \\ 0 & 1 \end{pmatrix} M^{NL}(x^{L_2} - x^{L_1}) \begin{pmatrix} 1 & \dfrac{-Q_0^{L_1}}{2(H_0^{L_1} - z^{L_1})} \\ 0 & 1 \end{pmatrix} M^{NL}(x^{L_1} - x^U)$$
$$= M^{NL}(x^M - x^U) + s^{L_1} M^{SL}(x^{L_1}) + s^{L_2} M^{SL}(x^{L_2}) - s^{L_1} s^{L_2} M^{CE} \tag{41}$$

Here, $M^{NL}(x^M - x^U)$ and $M^{SL}(x^{L_i})$ $(i = 1,2)$ are obtained from Eqs. (8) and (10), and

$$M^{CE} = \frac{g}{2\sqrt{(H_0^{L_1} - z^{L_1})(H_0^{L_2} - z^{L_2})}} \times \begin{pmatrix} Z^2 \sinh(\mu l_1) \sinh(\mu l_2) \cosh(\mu l_3) & -Z \cosh(\mu l_1) \sinh(\mu l_2) \cosh(\mu l_3) \\ -Z^3 \sinh(\mu l_1) \sinh(\mu l_2) \sinh(\mu l_3) & Z^2 \cosh(\mu l_1) \sinh(\mu l_2) \sinh(\mu l_3) \end{pmatrix} \tag{42}$$

represents the coupling effect of the double leaks, where $l_1 = x^{L_1}$, $l_2 = x^{L_2} - x^{L_1}$, and $l_3 = x^M - x^{L_2}$. Therefore, Eq. (25) is derived.

Appendix III. Time Reversal in the Frequency Domain

The head in the frequency domain is derived from a discrete Fourier transform (denoted by $\mathcal{F}_\omega$)

$$h(\omega) = \mathcal{F}_\omega(H(t)) = \sum_{t=-T}^{T} H(t) e^{-i\omega t} \tag{43}$$

where $H(t)$ is the head in the time domain. The conjugate of Eq. (43) is

$$h^c(\omega) = \sum_{t=-T}^{T} H(t) e^{i\omega t} \underline{\underline{t' = -t}} \sum_{t'=T}^{-T} H(-t') e^{-i\omega t'} = \sum_{t'=-T}^{T} H(-t') e^{-i\omega t'} = \mathcal{F}_\omega(H(-t)) \tag{44}$$

which implies that the conjugate operation in the frequency domain corresponds to the time reversal in the time domain.

Acknowledgments

The work described in this paper was supported by the research grants from the Research Grant Council of the Hong Kong SAR, China (Project No. T21-602/15R). The authors acknowledge Duncan A. McInnis, Bryan Karney, Fedi Zouari, Alireza Keramat, Moez Louati, and Jingrong Lin for their helpful comments and discussions.

Notation

The following symbols are used in this paper:

A = pipe area;
a = wave speed;
B = output function of MFP;
f = Darcy–Weisbach friction factor;
g = gravitational acceleration;
h = complex head oscillation;
M = transfer matrix;
$\mathbf{n}$ = measurement noise;
Q_0^L, H_0^L = steady-state discharge and head of leak;
q = complex discharge oscillation;
R = frictional resistance;
s^L = lumped leak parameter;
x^L = leak location;
x^M = measurement station coordinate;
Z = characteristic impedance;
z^L = pipe elevation at leak;
$\Delta\mathbf{h}$ = head difference;
μ = propagation function;
Σ (σ^2) = covariance matrix (variance) of noise.
ω = angular frequency; and
ω_{th} = resonant frequency.

Superscripts

c = complex conjugate;
D = downstream node;
H = conjugate transpose;
L = leak;
M = measurement;
NL = no leak;
SL = single leak; and
U = upstream node.

References

Baggeroer, A. B., W. A. Kuperman, and P. N. Mikhalevsky. 1993. "An overview of matched field methods in ocean acoustics." *IEEE J. Oceanic Eng.* 18 (4): 401–424.

Brunone, B. 1999. "Transient test-based technique for leak detection in outfall pipes." *J. Water Resour. Plann. Manage.* 125 (5): 302–306. https://doi.org/10.1061/(ASCE)0733-9496(1999)125:5(302).

Brunone, B., and M. Ferrante. 2001. "Detecting leaks in pressurised pipes by means of transients." *J. Hydraul. Res.* 39 (5): 539–547. https://doi.org/10.1080/00221686.2001.9628278.

Chaudhry, M. H. 2014. *Applied hydraulic transients*, 3rd ed. New York: Springer.

Colombo, A. F., P. Lee, and B. W. Karney. 2009. "A selective literature review of transient-based leak detection methods." *J. Hydro-Environ. Res.* 2 (4): 212–227. https://doi.org/10.1016/j.jher.2009.02.003.

Corciulo, M., P. Roux, M. Campillo, D. Dubucq, and W. A. Kuperman. 2012. "Multiscale matched-field processing for noise-source localization in exploration geophysics." *Geophysics*. 77 (5): KS33–KS41. https://doi.org/10.1190/geo2011-0438.1.

Covas, D., and H. Ramos. 2010. "Case studies of leak detection and location in water pipe systems by inverse transient analysis." *J. Water Resour. Plann. Manage.* 136 (2): 248–257. https://doi.org/10.1061/(ASCE)0733-9496(2010)136:2(248).

Covas, D., H. Ramos, and A. B. De Almeida. 2005a. "Standing wave difference method for leak detection in pipeline systems." *J. Hydraul. Eng.* 131 (12): 1106–1116. https://doi.org/10.1061/(ASCE)0733-9429(2005)131:12(1106).

Covas, D., H. Ramos, N. Graham, and C. Maksimovic. 2005b. "Application of hydraulic transients for leak detection in water supply systems." *Water Sci. Technol. Water Supply* 4 (5–6): 365–374.

Ferrante, M., and B. Brunone. 2003. "Pipe system diagnosis and leak detection by unsteady-state tests. 1. Harmonic analysis." *Adv. Water Resour.* 26 (1): 95–105. https://doi.org/10.1016/S0309-1708(02)00101-X.

Ferrante, M., B. Brunone, S. Meniconi, B. W. Karney, and C. Massari. 2014. "Leak size, detectability and test conditions in pressurized pipe systems." *Water Resour. Manage.* 28 (13): 4583–4598. https://doi.org/10.1007/s11269-014-0752-6.

Hall, J. S., and J. E. Michaels. 2010. "Minimum variance ultrasonic imaging applied to an in situ sparse guided wave array." *IEEE Trans. Ultrason. Ferroelectr. Freq. Control.* 57 (10): 2311–2323. https://doi.org/10.1109/TUFFC.2010.1692.

Hwang, Y. F., W. K. Bonness, and S. A. Hambric. 2009. "Comparison of semi-empirical models for turbulent boundary layer wall pressure spectra." *J. Sound Vibr.* 319 (1): 199–217. https://doi.org/10.1016/j.jsv.2008.06.002.

Jensen, F. B., W. A. Kuperman, M. B. Porter, and H. Schmidt. 2000. *Computational ocean acoustics*. New York: Springer.

Kashima, A., P. J. Lee, M. S. Ghidaoui, and M. Davidson. 2013. "Experimental verification of the kinetic differential pressure method for flow measurements." *J. Hydraul. Res.* 51 (6): 634–644. https://doi.org/10.1080/00221686.2013.818583.

Kessy, A., A. Lewin, and K. Strimmer. 2018. "Optimal whitening and decorrelation." *Am. Statistician.* 1–6. https://doi.org//10.1080/00031305.2016.1277159.

Khazaie, S., X. Wang, and P. Sagaut. 2016. "Localization of random acoustic sources in an inhomogeneous medium." *J. Sound Vibr.* 384: 75–93. https://doi.org//10.1016/j.jsv.2016.08.004.

Krim, H., and M. Viberg. 1996. "Two decades of array signal processing research." *IEEE Signal Process. Mag.* 13 (4): 67–94. https://doi.org//10.1109/79.526899.

Kuperman, W. A., and J. F. Lynch. 2004. "Shallow-water acoustics." *Phys. Today.* 57 (10): 55–61. https://doi.org//10.1063/1.1825269.

Lee, P. J., M. F. Lambert, A. R. Simpson, J. P. Vítkovský, and J. Liggett. 2006. "Experimental verification of the frequency response method for pipeline leak detection." *J. Hydraul. Res.* 44 (5): 693–707. https://doi.org//10.1080/00221686.2006.9521718.

Lee, P. J., J. P. Vítkovský, M. F. Lambert, A. R. Simpson, and J. A. Liggett. 2003. "Frequency response coding for the location of leaks in single pipeline systems." In *Int. Conf. on Pumps, Electromechanical Devices and Systems Applied to Urban Water Management*, 2–25. Valencia, Spain: IAHR and IHRA.

Lee, P. J., J. P. Vítkovský, M. F. Lambert, A. R. Simpson, and J. A. Liggett. 2005a. "Frequency domain analysis for detecting pipeline leaks." *J. Hydraul. Eng.* 131 (7): 596–604. https://doi.org//10.1061/(ASCE)0733-9429(2005)131:7(596).

Lee, P. J., J. P. Vítkovský, M. F. Lambert, A. R. Simpson, and J. A. Liggett. 2005b. "Leak location using the pattern of the frequency response diagram in pipelines: A numerical study." *J. Sound Vibr.* 284 (3): 1051–1073. https://doi.org//10.1016/j.jsv.2004.07.023.

Liggett, J. A., and L.-C. Chen. 1994. "Inverse transient analysis in pipe networks." *J. Hydraul. Eng.* 120 (8): 934–955. https://doi.org//10.1061/(ASCE)0733-9429(1994)120:8(934).

Liou, J. C. 1998. "Pipeline leak detection by impulse response extraction." *J. Fluids Eng.* 120 (4): 833–838. https://doi.org//10.1115/1.2820746.

Mpesha, W., S. L. Gassman, and M. H. Chaudhry. 2001. "Leak detection in pipes by frequency response method." *J. Hydraul. Eng.* 127 (2): 134–147. https://doi.org//10.1061/(ASCE)0733-9429(2001)127:2(134).

Picinbono, B. 1996. "Second-order complex random vectors and normal distributions." *IEEE Trans. Signal Process.* 44 (10): 2637–2640. https://doi.org//10.1109/78.539051.

Rubio Scola, I., G. Besançon, and D. Georges. 2016. "Blockage and leak detection and location in pipelines using frequency response optimization." *J. Hydraul. Eng.* 143 (1): 04016074. https://doi.org//10.1061/(ASCE)HY.1943-7900.0001222.

Sattar, A. M., and M. H. Chaudhry. 2008. "Leak detection in pipelines by frequency response method." Supplement, *J. Hydraul. Res.* 46 (S1): 138–151. https://doi.org//10.1080/00221686.2008.9521948.

Schantz, C., B. Sennett, J. Donnal, M. Gillman, and S. Leeb. 2014. "Non-intrusive load monitoring for water (waterNILM)." *WIT Trans. Built Environ.* 139: 103–114.

Stephens, M. L. 2008. "Transient response analysis for fault detection and pipeline wall condition assessment in field water transmission and distribution pipelines and networks." Ph.D. thesis, School of Civil, Environmental and Mining Engineering, Univ. of Adelaide.

Taghvaei, M., S. B. M. Beck, and J. B. Boxall. 2010. "Leak detection in pipes using induced water hammer pulses and cepstrum analysis." *Int. J. COMADEM.* 13 (1): 19.

Tippmann, J. D., X. Zhu, and F. Lanza di Scalea. 2015. "Application of damage detection methods using passive reconstruction of impulse response functions." *Philos. Trans. R. Soc. London A.* 373 (2035): 20140070. https://doi.org//10.1098/rsta.2014.0070.

Tolstoy, A., K. V. Horoshenkov, and M. T. Bin Ali. 2009. "Detecting pipe changes via acoustic matched field processing." *Appl. Acoust.* 70 (5): 695–702. https://doi.org//10.1016/j.apacoust.2008.08.007.

Tolstoy, A. I. 2010. "Waveguide monitoring (such as sewer pipes or ocean zones) via matched field processing." *J. Acoust. Soc. Am.* 128 (1): 190–194. https://doi.org//10.1121/1.3436521.

Turek, G., and W. A. Kuperman. 1997. "Applications of matched-field processing to structural vibration problems." *J. Acoust. Soc. Am.* 101 (3): 1430–1440. https://doi.org//10.1121/1.418168.

Vítkovský, J. P., A. R. Simpson, and M. F. Lambert. 2000. "Leak detection and calibration using transients and genetic algorithms." *J. Water Resour. Plann. Manage.* 126 (4): 262–265. https://doi.org//10.1061/(ASCE)0733-9496(2000)126:4(262).

Wang, X., and M. Ghidaoui. 2017. "Matched-field processing method for leak detection in a pipe." In *Proc., 37th IAHR World Congress*. Kuala Lumpur, Malaysia.

Wang, X., B. Quost, J.-D. Chazot, and J. Antoni. 2016a. "Estimation of multiple sound sources with data and model uncertainties using the EM and evidential EM algorithms." *Mech. Syst. Signal Process.* 66–67, 159–177. https://doi.org//10.1016/j.ymssp.2015.06.011.

Wang, X., B. Quost, J.-D. Chazot, and J. Antoni. 2016b. "Iterative beamforming for identification of multiple broadband sound sources." *J. Sound Vibr.* 365: 260–275. https://doi.org//10.1016/j.jsv.2015.11.036.

Wang, X.-J., M. F. Lambert, A. R. Simpson, J. A. Liggett, and J. P. Vítkovský. 2002. "Leak detection in pipelines using the damping of fluid transients." *J. Hydraul. Eng.* 128 (7): 697–711. https://doi.org//10.1061/(ASCE)0733-9429(2002)128:7(697).

Wylie, E. B., and V. L. Streeter. 1978. *Fluid transients*. New York: McGraw-Hill.